Supporting Information for

Ultralow-Concentration Electrolyte for Na-Ion Batteries

Yuqi Li,[‡,⊥,†] *Yang Yang,*[‡,⊥,†] *Yaxiang Lu,*[*,‡,§] *Quan Zhou,*[‡,⊥,§] *Xingguo Qi,*[‡,⊥,§] *Qingshi Meng,*[‡,⊥,§] *Xiaohui Rong,*[‡] *Liquan Chen,*[‡,⊥,§] *and Yong-Sheng Hu*[*,‡,⊥,§]

[‡]Key Laboratory for Renewable Energy, Beijing Key Laboratory for New Energy Materials and Devices, Beijing National Laboratory for Condensed Matter Physics, Institute of Physics, Chinese Academy of Sciences, Beijing 100190, China

[⊥]College of Materials Science and Optoelectronic Technology, University of Chinese Academy of Sciences, Beijing 100049, China

[§]Yangtze River Delta Physics Research Center Co. Ltd., Liyang 213300, China

Corresponding Author

*E-mail: yxlu@iphy.ac.cn; yshu@iphy.ac.cn.

Experimental Procedures

Materials and full cells:

The disordered carbon anode materials and layered O3-$Na[Cu_{1/9}Ni_{2/9}Fe_{1/3}Mn_{1/3}]O_2$ cathode materials were synthesized by high-temperature calcination according to the early report.[1] The composition of the electrodes was 90 wt.% active materials, 5 wt.% Super P, and 5 wt.% polyvinylidene fluoride (PVDF). The electrode slurries were casted on Al foil, followed by a drying process under vacuum. The electrolyte used for the full cells is *x* M (mol/L) $NaPF_6$ (Kishida Chemical Co., Ltd., 99%) dissolved in ethyl carbonate (EC)/propylene carbonate (PC) (1:1 vol.%) (Shandong Hirong power supply material Co., Ltd., 99.99%) without any functional additives. All the electrolytes were prepared and dried using molecular sieves (4 Å) in a glove box under high-purity argon gas. The amount of electrolyte used for a CR2032 coin-type cell is 200 μL and glass fiber (Whatman GF/D) was utilized as the separator. Aluminized battery shells were used for high temperature tests. The mass loadings of the anode and cathode are about 7 and 17 mg/cm^2 (cathode mass is limited), respectively.

Materials characterization:

Pt electrode equipment with a specific conductivity constant (Shanghai Russell Technology Co., Ltd.) was used to measure the ionic conductivities of the electrolytes. The conductivity constant should be predetermined using 1 M aqueous KCl standard solution at 25 °C. The ionic conductivities of the electrolytes were obtained from electrochemical impedance spectroscopy (EIS) using electrochemical workstation (IM6e Zahner) in the oven at set temperature. The viscosities of the electrolytes were measured from the Anton Paar MCR502 rheometer.

Electrochemical measurements and electrode characterization:

The cells were placed at oven thermostat in different temperature states. The charge and discharge tests of full cells were performed on the Land CT2001A battery test systems (Wuhan, China), cycled in the voltage range of 1.0-4.0 V at different current rates (1*C* = 100 mA/g). Note that the small current activation processes before the cycling tests are not shown in Figure 1c, 2b, S3, S4 and S6. The surface chemical state was determined by X-ray photoelectron spectroscopy (XPS) using the Thermo Scientific ESCALAB 250 Xi spectrometer with Mg/Al Kα X-ray source. All spectra were calibrated with the C 1s photoemission peak at 284.8 eV to correct for the charging effect. For the ex situ measurements, the electrode disassembled from the coin cell in an argon-filled glove box was washed in dimethyl carbonate (DMC) repeatedly followed by a drying processing in an argon-filled transferred tube.

Selected ionic conductivity and viscosity data:

25 °C: 5.64 mS/cm@0.3 M, 8.69 mS/cm@1 M vs 0 °C: 3.45 mS/cm@0.3 M, 5.26 mS/cm@1 M

25 °C: 3.46 mPa·S@0.3 M, 6.48 mPa·S@1 M vs 0 °C: 6.62 mPa·S@0.3 M, 15.2 mPa·S@1 M

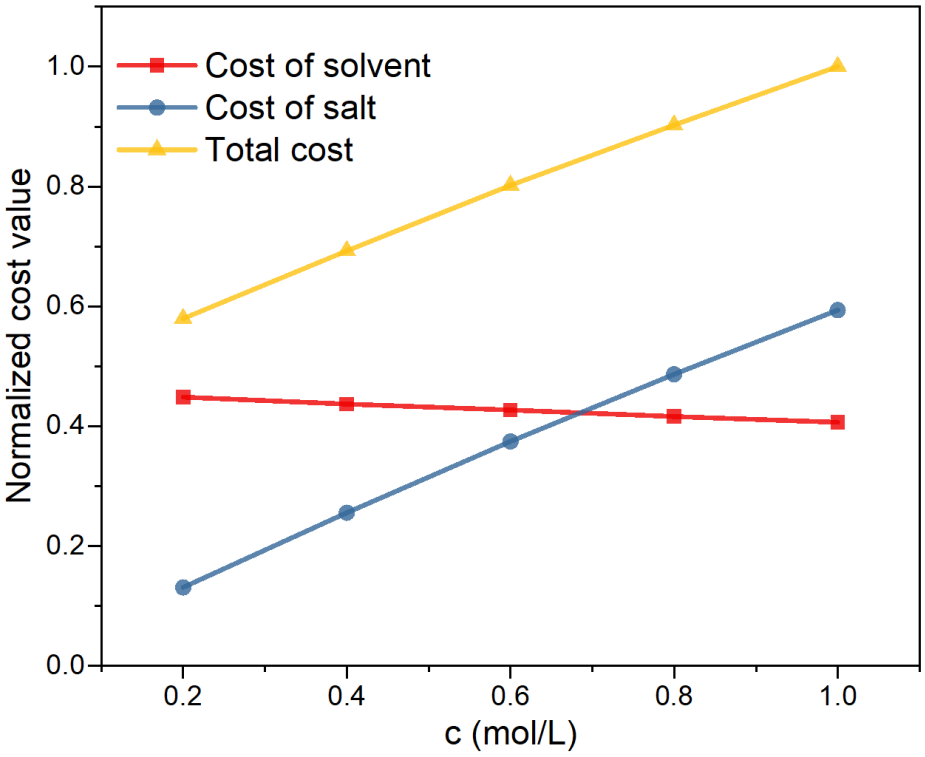

Figure S1. Predicted costs (per unit mass) of $NaPF_6$ in EC/PC electrolytes with different concentrations (suppose the cost of salt is eleven times higher than that of the solvent and make normalization based on total cost maximum).

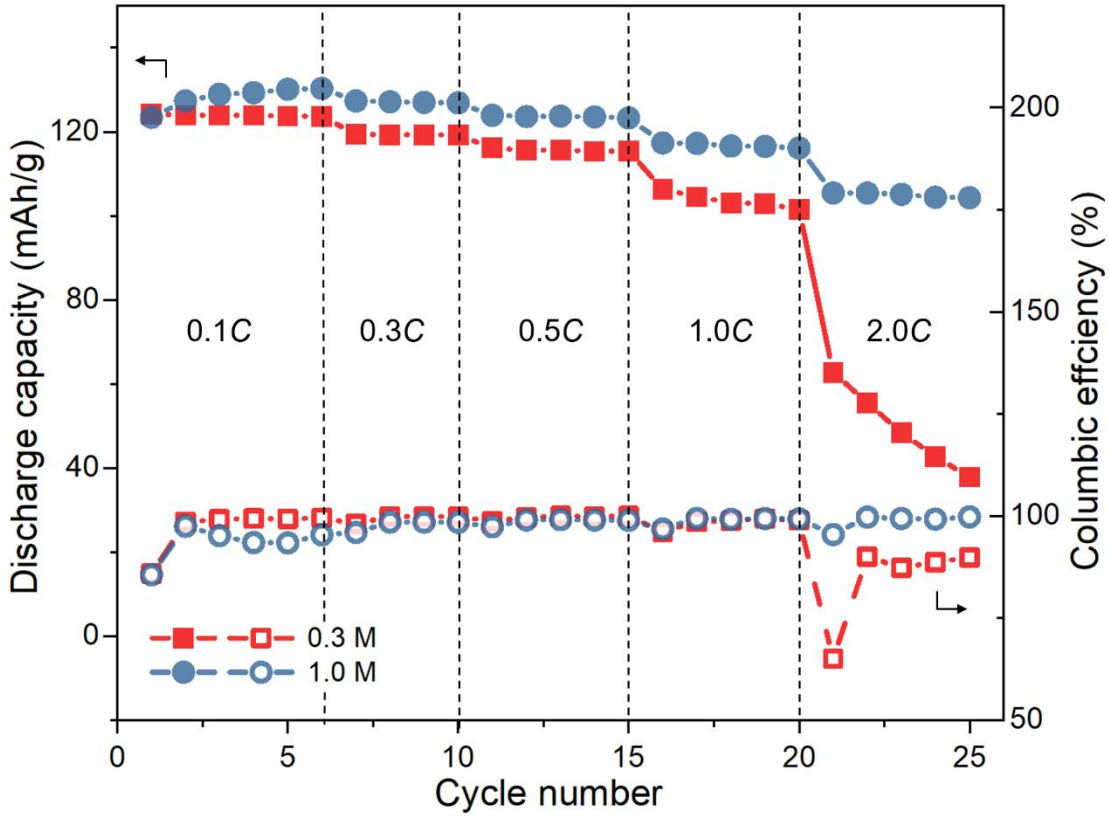

Figure S2. Rate performance of Na-ion full cells using 0.3 M or 1 M $NaPF_6$ in EC/PC electrolyte from 0.1*C* to 2*C* at 25 °C. There is a significant capacity loss during cycling at 2*C* due to the concentration polarization in the 0.3 M electrolyte.

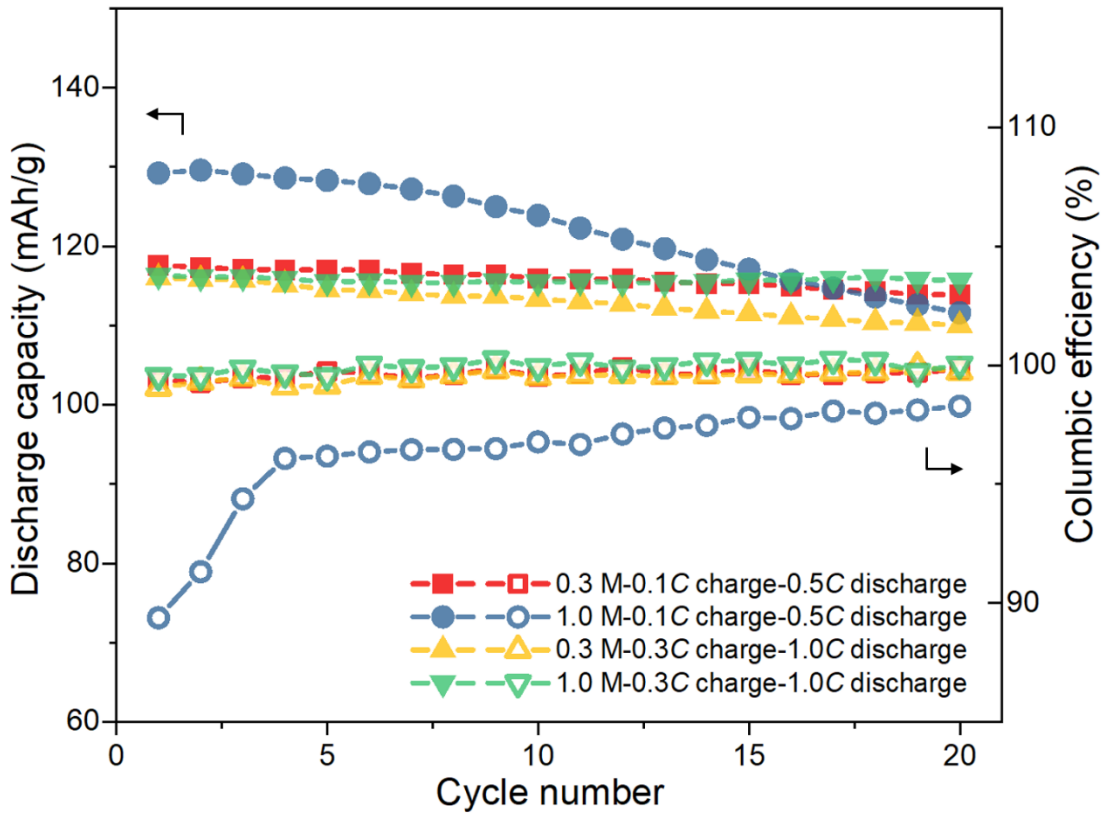

Figure S3. Rate performance (asymmetric charge-discharge cycling tests) of Na-ion full cells using 0.3 M or 1 M $NaPF_6$ in EC/PC electrolyte at 25 °C.

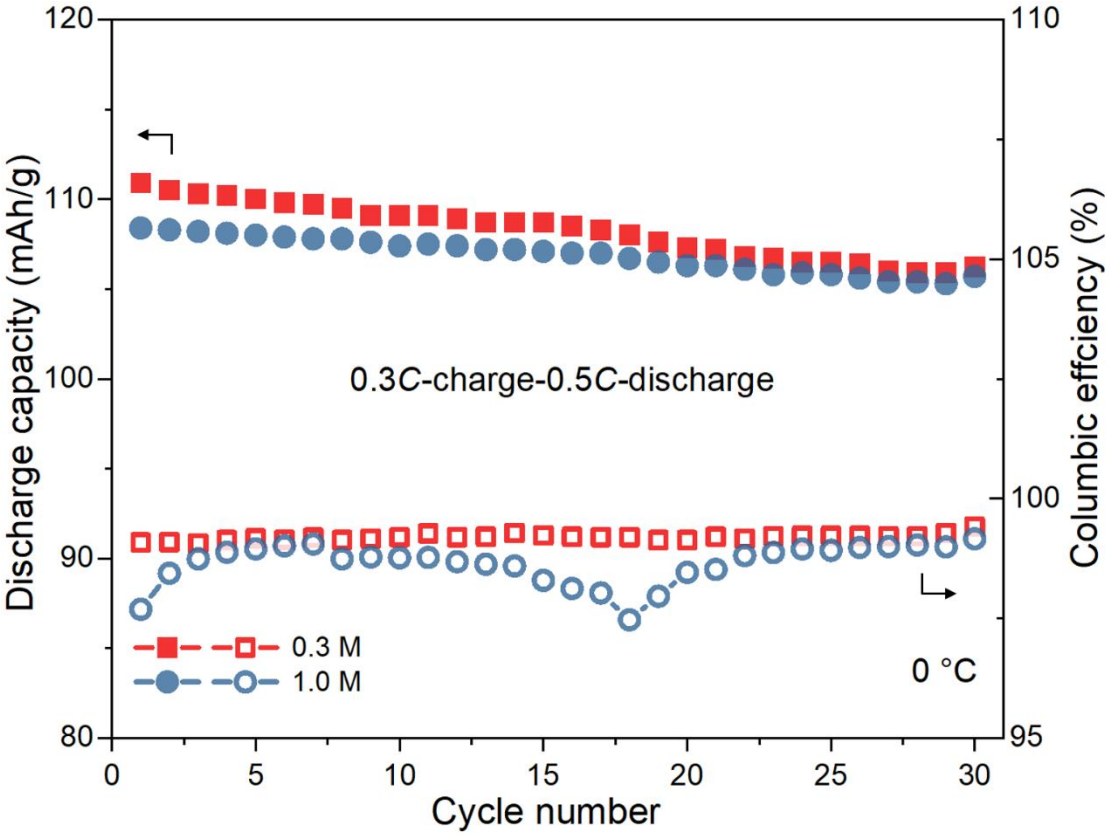

Figure S4. Rate performance (asymmetric charge-discharge cycling tests) of Na-ion full cells using 0.3 M or 1 M $NaPF_6$ in EC/PC electrolyte at 0 °C.

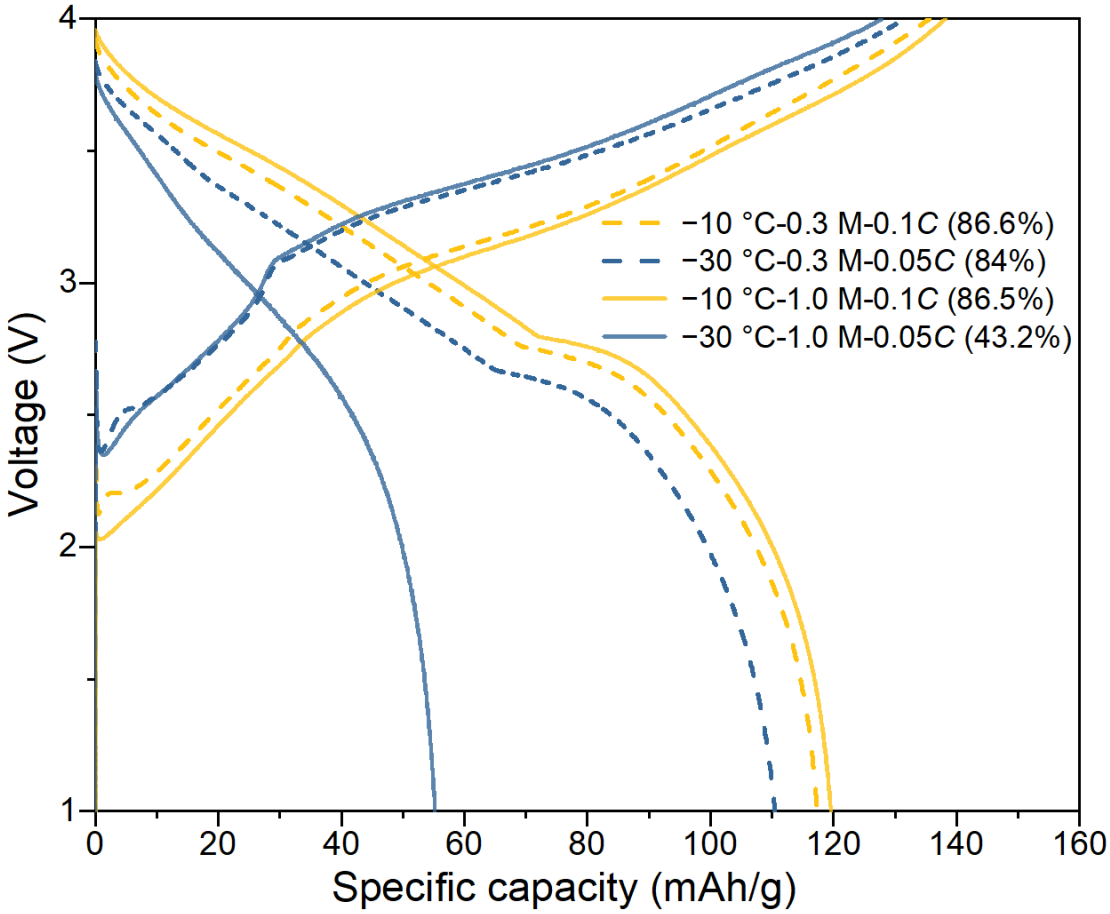

Figure S5. Galvanostatic initial discharge/charge curves of Na-ion full cells using 0.3 M or 1 M $NaPF_6$ in EC/PC electrolyte at −10 °C and −30 °C. The related ICEs are noted in parentheses.

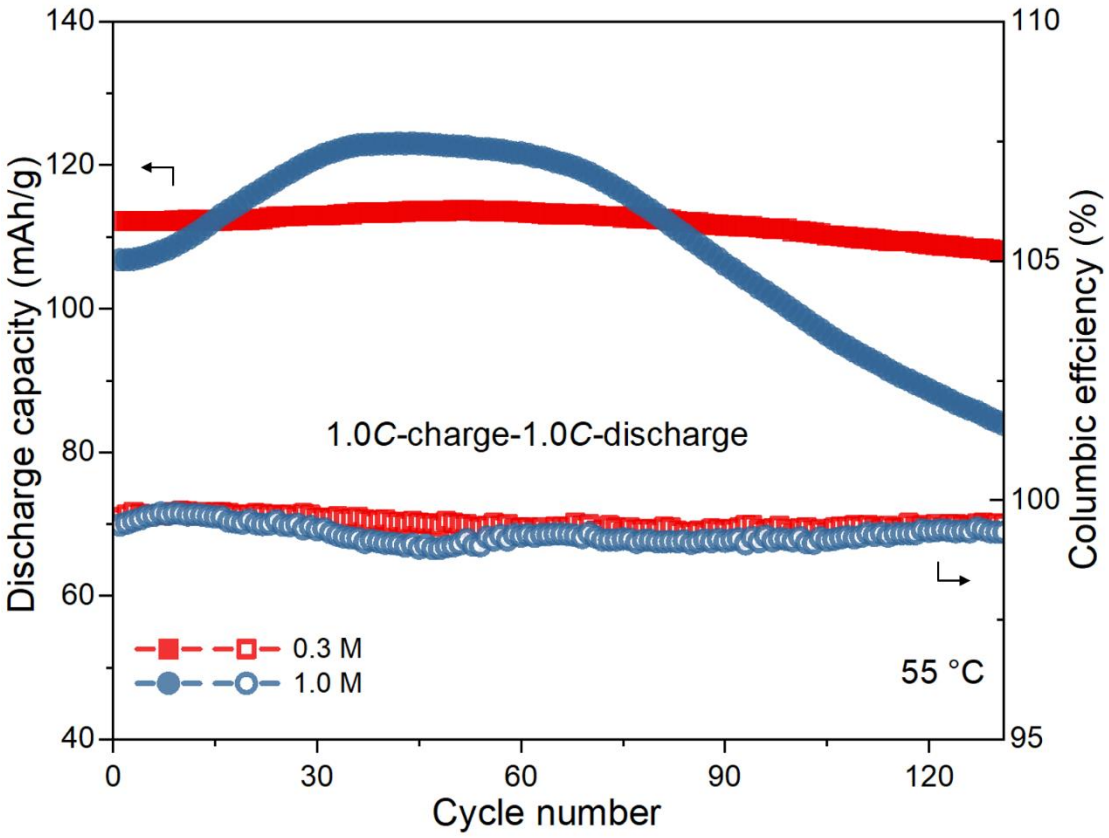

Figure S6. Cyclic capability at a current rate of 1*C* of Na-ion full cells using 0.3 M or 1 M $NaPF_6$ in EC/PC electrolyte at 55 °C.

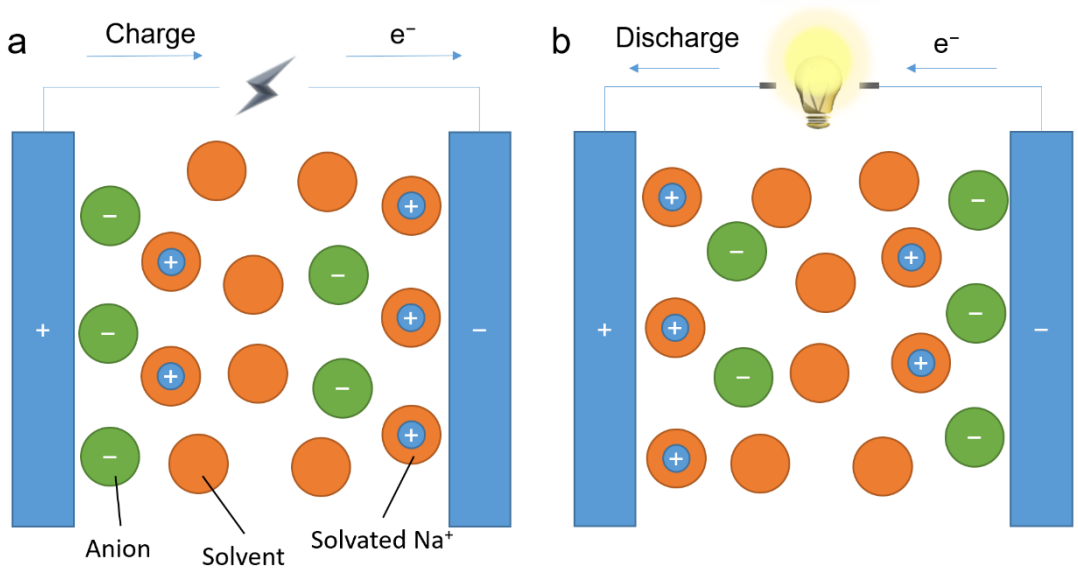

Figure S7. A schematic illustration of the formation of electrical double layers and concentration gradients during the charging (a) or discharging (b) of NIBs.[2]

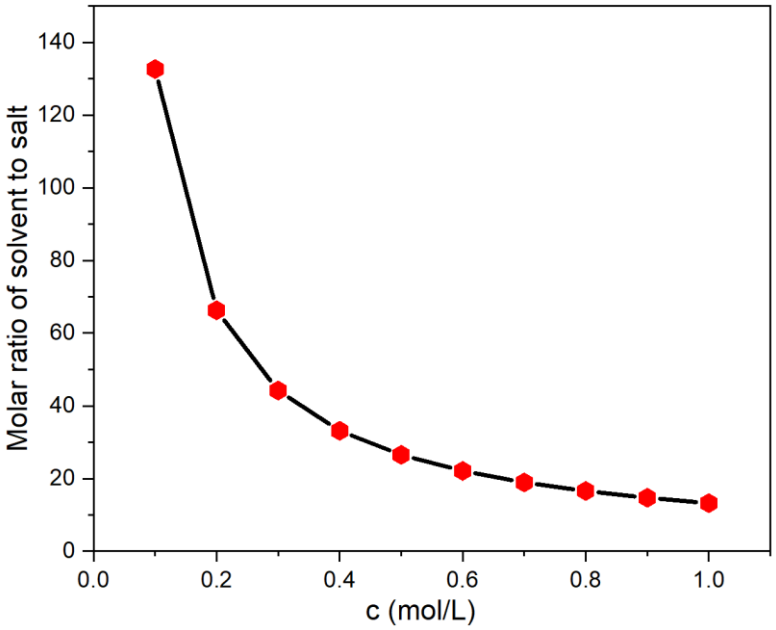

Figure S8. Relation curve of the molar ratio of solvent to salt and the concentration of $NaPF_6$ in EC/PC electrolyte.[3-4]

Insights on the novel dilute electrolyte chemistry:

Normally, the organic composition of SEI in NIBs is less than that of LIBs,[5] and thus more elastic organic components[6] are needed considering the irregular surface of disordered carbon and poor ionic conductivity of NaF. Increasing the molar ratio of solvent to salt can exactly improve the ratio of organic components (Figure S8). The organic layer can be permeable to electrolytes as a thick extended outer layer[2, 7-8] and even partial soluble components can form the effective conductive network[6, 9] to compensate the concentration polarization. According to the electrical double layer theory (Figure S7),[2] fast charge/discharge reaction in the 1.0 M electrolyte may provide the similar effect using the 0.3 M electrolyte by increasing the organic components but decreasing the inorganic components. The novel dilute electrolyte chemistry needs to be further explored which is currently in progress.

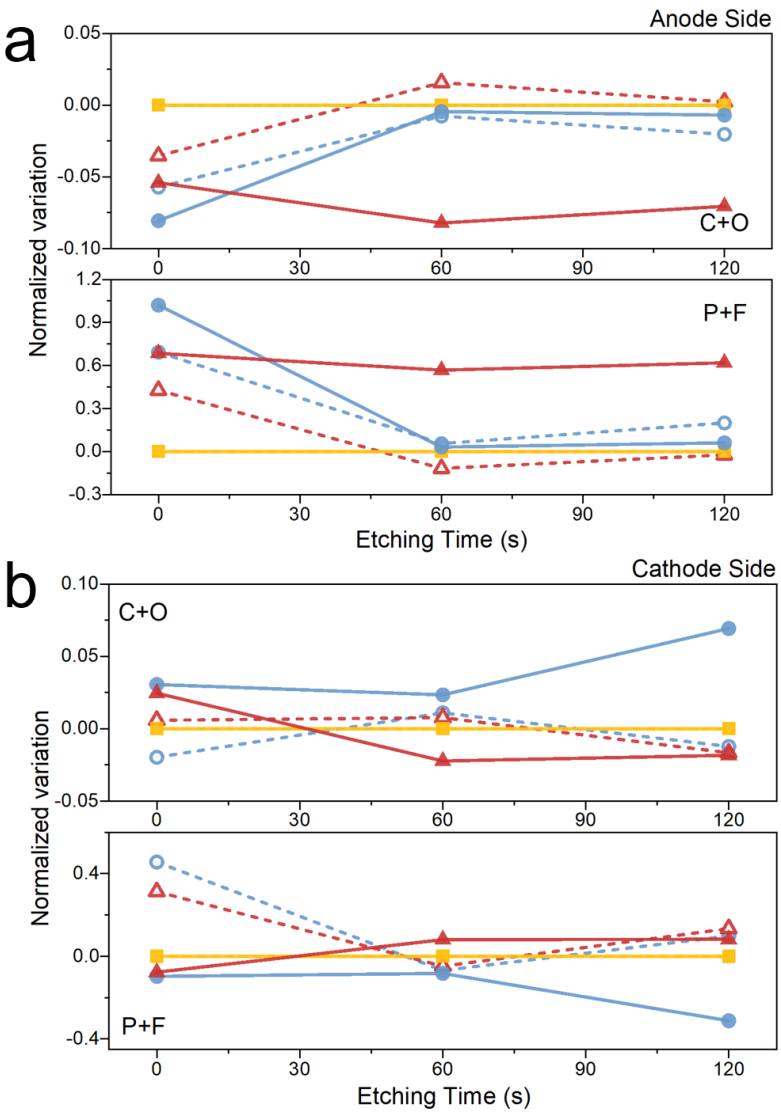

Figure S9. Variations in the atomic ratios of C (C1s spectra) plus O (O1s spectra) and P (P 2p spectra) plus F (F 1s spectra) elements detected at (a) the SEI films of carbon anodes and (b) the CEI films of layered oxide cathodes formed at the different temperature (the component data collected at 25 °C as the zero references).

Table S1. Detailed XPS data detected on anode sides (the Na signals were excluded).

C (C1s, %)	E-0s	E-60s	E-120s
25°C-0.3M	57.37	56.01	66.77
25°C-1.0M	53.39	58.74	68.79
0°C-0.3M	56.7	68.63	74.05
0°C-1.0M	59.56	62.68	70.96
55°C-0.3M	43.94	56.38	64.16
55°C-1.0M	44.33	34.13	51.99

O (O1s, %)	E-0s	E-60s	E-120s
25°C-0.3M	35	32.11	24
25°C-1.0M	39.3	28.61	20.97
0°C-0.3M	30.39	18.82	14.87
0°C-1.0M	25.66	24.28	18.17
55°C-0.3M	45.17	33.12	26.82
55°C-1.0M	43.35	46.04	31.44

P (P2p, %)	E-0s	E-60s	E-120s
25°C-0.3M	0.3	0.32	0.41
25°C-1.0M	0.68	0.52	0.99
0°C-0.3M	1.06	0.79	0.76
0°C-1.0M	0.7	0	0
55°C-0.3M	0.19	0.93	0.5
55°C-1.0M	3.72	3.31	1.55

F (F1s, %)	E-0s	E-60s	E-120s
25°C-0.3M	7.32	11.57	8.82
25°C-1.0M	6.64	12.13	9.25
0°C-0.3M	11.84	11.76	10.32
0°C-1.0M	14.09	13.05	10.87
55°C-0.3M	10.69	9.57	8.52
55°C-1.0M	8.61	16.52	15.02

Table S2. Detailed XPS data detected on cathode sides (the Na, Ni, Cu, Fe, Mn signals were excluded).

C (C1s, %)	E-0s	E-60s	E-120s
25°C-0.3M	56.37	78.22	76.21
25°C-1.0M	70.56	73.14	76.31
0°C-0.3M	71.42	81	79.3
0°C-1.0M	72.54	71.43	75.32
55°C-0.3M	71.87	76.28	76.04
55°C-1.0M	62.68	72.59	76.08

O (O1s, %)	E-0s	E-60s	E-120s
25°C-0.3M	14.03	7.96	12.82
25°C-1.0M	5.28	4.96	5.54
0°C-0.3M	7.47	6.12	8.64
0°C-1.0M	5.62	8.5	12.2
55°C-0.3M	9.08	10.56	11.51
55°C-1.0M	15.02	3.77	4.27

P (P2p, %)	E-0s	E-60s	E-120s
25°C-0.3M	0.51	0.34	0.33
25°C-1.0M	0.28	0.71	0.69
0°C-0.3M	0.34	0.33	0.97
0°C-1.0M	0.32	0.26	0.68
55°C-0.3M	0.63	0.51	0.73
55°C-1.0M	0.97	0.49	1.06

F (F1s, %)	E-0s	E-60s	E-120s
25°C-0.3M	29.1	13.48	10.65
25°C-1.0M	23.9	21.19	17.47
0°C-0.3M	20.78	12.54	11.09
0°C-1.0M	21.51	19.82	11.81
55°C-0.3M	18.42	12.65	11.72
55°C-1.0M	21.34	23.16	18.59

The present forms of the P and F are mainly NaF, Na_xPOF_y and Na_xPF_y from the F 1s and P 2p X-ray photoelectron spectra.

References

1. Mu, L.; Qi, X.; Hu, Y.-S.; Li, H.; Chen, L.; Huang, X., Electrochemical properties of novel O3-$NaCu_{1/9}Ni_{2/9}Fe_{1/3}Mn_{1/3}O_2$ as cathode material for sodium-ion batteries. *Energy Storage Science and Technology* **2016,** *5* (3), 324.

2. Zhou, Y.; Su, M.; Yu, X.; Zhang, Y.; Wang, J.-G.; Ren, X.; Cao, R.; Xu, W.; Baer, D. R.; Du, Y.; Borodin, O.; Wang, Y.; Wang, X.-L.; Xu, K.; Xu, Z.; Wang, C.; Zhu, Z., Real-time mass spectrometric characterization of the solid–electrolyte interphase of a lithium-ion battery. *Nature Nanotechnology* **2020,** *15* (3), 224-230.

3. Xiao, L.; Zeng, Z.; Liu, X.; Fang, Y.; Jiang, X.; Shao, Y.; Zhuang, L.; Ai, X.; Yang, H.; Cao, Y.; Liu, J., Stable Li Metal Anode with "Ion–Solvent-Coordinated" Nonflammable Electrolyte for Safe Li Metal Batteries. *ACS Energy Letters* **2019,** *4* (2), 483-488.

4. Zhou, L.; Cao, Z.; Wahyudi, W.; Zhang, J.; Hwang, J.-Y.; Cheng, Y.; Wang, L.; Cavallo, L.; Anthopoulos, T.; Sun, Y.-K.; Alshareef, H. N.; Ming, J., Electrolyte Engineering Enables High Stability and Capacity Alloying Anodes for Sodium and Potassium Ion Batteries. *ACS Energy Letters* **2020**, 766-776.

5. Komaba, S.; Murata, W.; Ishikawa, T.; Yabuuchi, N.; Ozeki, T.; Nakayama, T.; Ogata, A.; Gotoh, K.; Fujiwara, K., Electrochemical Na insertion and solid electrolyte interphase for hard-carbon electrodes and application to Na-Ion batteries. *Advanced Functional Materials* **2011,** *21* (20), 3859-3867.

6. Wang, L.; Menakath, A.; Han, F.; Wang, Y.; Zavalij, P. Y.; Gaskell, K. J.; Borodin, O.; Iuga, D.; Brown, S. P.; Wang, C.; Xu, K.; Eichhorn, B. W., Identifying the components of the solid–electrolyte interphase in Li-ion batteries. *Nature Chemistry* **2019,** *11* (9), 789-796.

7. Huang, W.; Attia, P. M.; Wang, H.; Renfrew, S. E.; Jin, N.; Das, S.; Zhang, Z.; Boyle, D. T.; Li, Y.; Bazant, M. Z.; McCloskey, B. D.; Chueh, W. C.; Cui, Y., Evolution of the Solid–Electrolyte Interphase on Carbonaceous Anodes Visualized by Atomic-Resolution Cryogenic Electron Microscopy. *Nano Letters* **2019,** *19* (8), 5140-5148.

8. He, M.; Guo, R.; Hobold, G. M.; Gao, H.; Gallant, B. M., The intrinsic behavior of lithium fluoride in solid electrolyte interphases on lithium. *Proceedings of the National Academy of Sciences* **2020,** *117* (1), 73.

9. Mogensen, R.; Brandell, D.; Younesi, R., Solubility of the Solid Electrolyte Interphase (SEI) in Sodium Ion Batteries. *ACS Energy Letters* **2016,** *1* (6), 1173-1178.